Johann Radon Institute for
Computational and Applied Mathematics
Austrian Academy of Sciences (ÖAW)

Detection of point-like scatterers using one type of scattered elastic waves

M. Sini, T.T. Nguyen

RICAM-Report 2011-27

Detection of point-like scatterers using one type of scattered elastic waves*

Drossos Gintides[1], Mourad Sini[2†]and Nguyen Trung Thành[2]
[1]National Technical University of Athens,
Zografou Campus, Zografou 15780 Athens, Greece.
Email address: dgindi@math.ntua.gr.
[2]Johann Radon Institute for Computational and Applied Mathematics (RICAM),
Austrian Academy of Sciences
Altenbergerstrasse 69, A-4040 Linz, Austria.
Email addresses: mourad.sini@oeaw.ac.at; trung-thanh.nguyen@oeaw.ac.at.

Abstract

In this paper, we are concerned with the detection of point-like obstacles using elastic waves. We show that one type of waves, either the P or the S scattered waves, is enough for localizing the points. We also show how the use of S incident waves gives better resolution than the P waves. These affirmations are demonstrated by several numerical examples using a MUSIC type algorithm.

Keywords: Elastic scattering, point-like scatterers, MUSIC algorithm.

1 Introduction

Let D_j, $j = 1, ..., M$, $M \in \mathbb{N}$, be bounded and open subsets of $\mathbb{R}^n$, $n = 2, 3$, such that $\mathbb{R}^n \setminus \overline{D_j}$ are connected and assume that they are disjoint. The boundary ∂D_j, $j = 1, ..., M$, of D_j is of class C^2 and the unit normal vector ν is directed into the exterior of D_j. Finally, we set $D := \cup_{j=1}^{M} D_j$. We denote by ρ the density function such that $\rho = 1$ in $\mathbb{R}^n \setminus \overline{D}$, continuous inside D and has a discontinuity across ∂D. We also denote by λ and μ the Lamé coefficients and we assume that those coefficients are constant in $\mathbb{R}^n$ and satisfy the conditions $\mu > 0$ and $2\mu + 3\lambda > 0$. We are concerned with the scattering problem of elastic waves by the obstacle D at a fixed frequency ω. Precisely, if u^i, which is a vector field satisfying $\mu \Delta u^i + (\lambda + \mu) \nabla \text{div } u^i + \omega^2 u^i = 0$ in $\mathbb{R}^n$, is the incident field, then the

*This report was accepted for publication in *Journal of Computational and Applied Mathematics, 2011.*
†Corresponding author

total field $u^t := u^i + u$, with $u \in C^2(\mathbb{R}^n \setminus \partial D)$ as the scattered field, is the solution to the following inhomogeneous problem associated with the Lamé system

$$\begin{cases} \mu\Delta u^t + (\lambda+\mu)\nabla \text{div } u^t + \omega^2\rho u^t = 0, \ \text{ in } \mathbb{R}^n \\ \lim\limits_{|x|\to\infty} |x|^{\frac{n-1}{2}}(\frac{\partial u_p}{\partial |x|} - ik_p u_p) = 0, \text{ and } \lim\limits_{|x|\to\infty} |x|^{\frac{n-1}{2}}(\frac{\partial u_s}{\partial |x|} - ik_s u_s) = 0, \end{cases} \tag{1}$$

where the last two limits are uniform in all directions $\hat{x} := \frac{x}{|x|} \in \mathbb{S}^{n-1}$ – the unit sphere in $\mathbb{R}^n$. Here, we denoted by $u_p := -k_p^{-2}\nabla \text{div } u$ to be the longitudinal (or the pressure) part of the field u and $u_s := -k_s^{-2}\text{curl curl } u$ to be the transversal (or the shear) part of the field u corresponding to the Helmholtz decomposition $u = u_p + u_s$. The constants $k_p := \frac{\omega}{\sqrt{2\mu+\lambda}}$ and $k_s := \frac{\omega}{\sqrt{\mu}}$ are known as the longitudinal and the transversal wavenumbers, respectively. It is well known that the scattering problem (1) is well posed, see for instance [16, 20, 21].

The scattered field u satisfies the following asymptotic expansion at infinity

$$u(x) := \frac{e^{i\kappa_p|x|}}{|x|^{\frac{n-1}{2}}} u_p^\infty(\hat{x}) + \frac{e^{i\kappa_s|x|}}{|x|^{\frac{n-1}{2}}} u_s^\infty(\hat{x}) + O(\frac{1}{|x|^{\frac{n+1}{2}}}), \ |x| \to \infty \tag{2}$$

uniformly in all directions $\hat{x} \in \mathbb{S}^{n-1}$, see [17] for instance. The fields $u_p^\infty(\hat{x})$ and $u_s^\infty(\hat{x})$ defined on $\mathbb{S}^{n-1}$ are called respectively the longitudinal and transversal parts of the far field pattern. The longitudinal part $u_p^\infty(\hat{x})$ is normal to $\mathbb{S}^{n-1}$ while the transversal part $u_s^\infty(\hat{x})$ is tangential to $\mathbb{S}^{n-1}$. Due to this property, they can be measured separately. Note that it is not necessarily true for near field measurements. In this case, see [6] for an approximate separation of these two components. Now, we specify the type of incident waves used in this work.

As usual in the scattering problems, we use plane waves as incident waves. For the Lamé system, they have the analytic forms

$$u^{i,p}(x,\theta) := \theta e^{i\kappa_p \theta\cdot x} \text{ and } u^{i,s}(x,\theta) := \theta^\perp e^{i\kappa_s\theta\cdot x}, \tag{3}$$

where $\theta^\perp$ is any vector in $\mathbb{S}^{n-1}$ orthogonal to θ. Remark that $u^{i,p}(\cdot,\theta)$ is normal to $\mathbb{S}^{n-1}$ and $u^{i,s}(\cdot,\theta)$ is tangential to $\mathbb{S}^{n-1}$.

Hence, we can define the matrix

$$(u^{i,p}, u^{i,s}) \mapsto F(u^{i,p}, u^{i,s}) := \begin{bmatrix} u_p^{\infty,p}(\cdot,\theta) & u_p^{\infty,s}(\cdot,\theta) \\ u_s^{\infty,p}(\cdot,\theta) & u_s^{\infty,s}(\cdot,\theta) \end{bmatrix} \tag{4}$$

where:

1. $(u_p^{\infty,p}(\cdot,\theta), u_s^{\infty,p}(\cdot,\theta))$ is the far field pattern associated with the pressure incident field $u^{i,p}(\cdot,\theta)$.

2. $(u_p^{\infty,s}(\cdot,\theta), u_s^{\infty,s}(\cdot,\theta))$ is the far field pattern associated with the shear incident field $u^{i,s}(\cdot,\theta)$.

In this paper, we are interested in the following inverse scattering problem: *From the knowledge of the matrix (4) for all directions $\hat{x}$ and θ in $\mathbb{S}^{n-1}$, determine D.*

Several works have been published regarding this inverse problem, see for instance [10, 11, 13] using the full matrix (4) for all directions $\hat{x}$ and θ in $\mathbb{S}^{n-1}$. For near field measurements, see [4, 5, 9, 15, 26]. We also mention the works [1, 3, 7, 18] regarding small obstacles and [6] for imaging extended obstacles.

We consider now the cavity problem

$$\begin{cases} \mu\Delta u + (\lambda+\mu)\nabla \mathrm{div}\, u + \omega^2 u = 0, \quad \text{in } \mathbb{R}^n \setminus \overline{D} \\ \sigma(u)\cdot\nu = -\sigma(u^i)\cdot\nu, \quad \text{on } \partial D \\ \lim\limits_{|x|\to\infty} |x|^{\frac{n-1}{2}}(\frac{\partial u_p}{\partial|x|} - ik_p u_p) = 0, \text{ and } \lim\limits_{|x|\to\infty} |x|^{\frac{n-1}{2}}(\frac{\partial u_s}{\partial|x|} - ik_s u_s) = 0, \end{cases} \tag{5}$$

where $\sigma(u)\cdot\nu := (2\mu\partial\nu + \lambda\nu\mathrm{div} + \mu\nu\times\mathrm{curl})u$. This problem is well posed, see [2, 20, 21], and we have a similar asymptotic behavior as (2). Hence, we can define the far field matrix as in (4). With this at hand, we state the similar inverse problem as for the inhomogeneous medium case.

The first uniqueness result for this problem was proved in [17]. It says that every *column* of the matrix (4) for all directions $\hat{x}$ and θ in $\mathbb{S}^{n-1}$, determines D. Sampling type methods for solving this obstacle inverse scattering problem have been developed by several authors, see [2, 8] using the full matrix (4) for all directions $\hat{x}$ and θ in $\mathbb{S}^{n-1}$.

We remark that in the above works, not only the information over all directions of incidence and observation, but also both pressure and shear parts of the far field pattern are needed. In [14], we proved that it is possible to reduce the amount of data for detecting D as follows:

Theorem 1.1. *Every component of the matrix (4) known for all directions $\hat{x}$ and θ in $\mathbb{S}^{n-1}$, determines D for the model* (5).

Remark that in Theorem 1.1, we need only the longitudinal part (or only the transverse part) of the far field pattern if we use longitudinal incident waves or transversal incident waves. The result in Theorem 1.1 is also valid for the inhomogeneous medium model (1). The proof is based on the asymptotic expansion of the singular solutions of the models in (1) and (5), see [25] for the impenetrable case and [24] for the penetrable case related to the scalar equations. The details will be written in a future work.

The objective of this paper is the following. Firstly, we would like to propose numerical methods corresponding to the uniqueness result in Theorem 1.1. Secondly, we would like to see whether the choice of the type of incident field is relevant or not. For this, we restrict ourselves to the case of point-like obstacles for which more explicit calculations can be done. Note that none of the known methods (iterative, sampling, probe, etc.) have been applied for detection by elastic waves using the reduced amount of data mentioned

in Theorem 1.1. To our knowledge, the only result considering the use of one type of elastic scattered waves for the detection is the one by Simonetti [27] who used P incident waves and the P part of the scattered waves to detect point-like obstacles. He showed by numerical results that MUSIC type algorithms achieved sub-wavelength resolution. However, no mathematical justification, as in Theorem 1.1 or in Theorem 3.1, was given there.

Using a MUSIC type algorithm, we show that indeed one type of waves is enough for the reconstruction. In addition, using S incident waves we obtain better resolution than when using P incident waves in the presence of noise. This can be explained by the fact that the S incident waves have shorter wavelengths than the P incident waves. We note that, since we make use of a weak scattering model to simulate the measured data, it is not physically meaningful to apply this model to the case of close scatterers. Therefore, the notion of resolution in this paper should be understood as the minimum distance between two point-like scatterers that can be resolved by the algorithm in the presence of measurement noise. That is, the resolution depends on the noise level. However, we should remark that this weak scattering assumption is merely for the simplicity of the forward modeling. In a future work, we will investigate the resolution of the MUSIC type algorithms using a more physically meaningful model which can be used also for close scatterers.

The rest of the paper is organized as follows. In section 2, we describe briefly the scattering of point-like obstacles including weak (Born) approximation. Section 3 is devoted to the MUSIC algorithms for scalar and elastic waves. Finally, section 4 shows numerical examples of the MUSIC algorithms and to confirm our discussions on the resolution limits.

2 Point-like obstacles

Consider M point-like scatterers located at $y_1, y_2, \ldots, y_M$ in $\mathbb{R}^n$. Suppose that they are illuminated by an incident plane elastic wave $u^i(x,\theta), x \in \mathbb{R}^n, \theta \in \mathbb{S}^{n-1}$. As described in the introduction, here $u^i(x,\theta) = u^{i,p}(x,\theta)$ or $u^i(x,\theta) = u^{i,s}(x,\theta)$.

As it is shown in [23], section 8.4, the total scalar field u^t corresponding to the scalar model (acoustic model for instance) is written as follows:

$$u^t(x) = u^i(x) + \sum_{m=1}^{M} \tau_m u^t(y_m)\Phi(x, y_m), \tag{6}$$

where u^i is the incident scalar field and Φ is the fundamental solution of the associated Helmholtz model. Equation (6) is obtained from the Lipmann-Schwinger equation by replacing the source, given by the density in each D_m, $m = 1, ..., M$, by $\tau_m \delta(y_m)$. Here, δ is the Dirac measure.

Following this approach, using the Lipmann-Schwinger equation corresponding to problem (1), under the assumption that the Lamé coefficients λ and μ are constant in $\mathbb{R}^n$, the

total vector field corresponding to the Lamé system can be described as follows

$$u^t(x) = u^i(x) + \sum_{m=1}^{M} \tau_m G(x, y_m) u^t(y_m), \tag{7}$$

where u^i is the incident vector field and G is the fundamental tensor associated with the Lamé system. The constant $\tau_m \in \mathbb{C}, \tau_m \neq 0$, represents the scattering strength of the m-th scatterer D_m.

2.1 Weak scattering approximation

The main difficulty in using the model (7) to generate the far field is the calculation of $u(y_j)$. This is due to the singularities of G on the points y_j, see [23] for more details. To avoid this, we use the weak scattering approximation. However, we should note that the MUSIC type algorithms are applicable for the nonlinear model (7) since the proofs of Theorem 4.1 of [19] and Theorem 3.1 are also valid for this case. For results using the scalar model (6), we refer the reader to [22]. A current work is being carried out for the elastic model (7) and we will discuss this in a future work.

Assume that there is no multiple scattering between the scatterers (Born approximation), then the scattered wave can be written in the form

$$u(x, \theta) = \sum_{m=1}^{M} \tau_m G(x, y_m) u^i(y_m, \theta), \tag{8}$$

by replacing in the right hand side of (7) u^t by u^i.

The asymptotic behavior of the Green tensor at infinity is given as follows

$$G(x, y_m) = a_p \hat{x} \otimes \hat{x} \frac{e^{ik_p|x|}}{|x|^{\frac{n-1}{2}}} e^{-ik_p \hat{x} \cdot y_m} + a_s (I - \hat{x} \otimes \hat{x}) \frac{e^{ik_s|x|}}{|x|^{\frac{n-1}{2}}} e^{-ik_s \hat{x} \cdot y_m} + O(|x|^{-\frac{n+1}{2}}), \tag{9}$$

with $\hat{x} = \frac{x}{|x|}$ and I being the identity matrix in $\mathbb{R}^n$, $a_p = \frac{k_p^2}{4\pi\omega^2}$ and $a_s = \frac{k_s^2}{4\pi\omega^2}$, see for instance [2].

It follows from (8) and (9) that the P and S parts of the far field pattern associated with the P incident wave $u^{i,p}$ are given by

$$u_p^{\infty,p}(\hat{x}, \theta) = a_p \sum_{m=1}^{M} \tau_m (\hat{x} \otimes \hat{x}) \cdot \theta e^{ik_p y_m \cdot (\theta - \hat{x})}, \tag{10}$$

$$u_s^{\infty,p}(\hat{x}, \theta) = a_s \sum_{m=1}^{M} \tau_m (I - \hat{x} \otimes \hat{x}) \cdot \theta e^{ik_p y_m \cdot \theta} e^{-ik_s y_m \cdot \hat{x}}. \tag{11}$$

Similarly, the P and S parts of the far field pattern associated with the S incident wave

$u^{i,s}$ can be written as

$$u_s^{\infty,p}(\hat{x},\theta) = a_p \sum_{m=1}^{M} \tau_m (\hat{x}\otimes\hat{x})\cdot\theta^{\perp} e^{ik_s y_m\cdot\theta} e^{-ik_p y_m\cdot\hat{x}}, \tag{12}$$

$$u_s^{\infty,s}(\hat{x},\theta) = a_s \sum_{m=1}^{M} \tau_m (I-\hat{x}\otimes\hat{x})\cdot\theta^{\perp} e^{ik_s y_m\cdot(\theta-\hat{x})}. \tag{13}$$

Here we have used the subscripts p and s to represent the P and S parts of the far field pattern and the superscripts p and s to represent the P and S incident waves, respectively.

3 MUSIC algorithms

The first MUSIC algorithm for determining the locations of point-like scatterers was firstly developed by Devaney [12] in 2000 using near field measurements of electromagnetic waves. So far, several works have been studying this type of algorithms for both near field and far field measurements and for different types of waves. For the elasticity, Ammari *et al.* [3] used the MUSIC algorithm with full Green's matrix as the measurements to reconstruct the locations of small inclusions and Simonetti [27] showed some numerical results using a MUSIC algorithm for only one part (S or P) of the scattered waves.

In this paper, we also use the MUSIC type algorithms for reconstructing the locations of the scatterers but using only one part of the far field patterns and one type of incident plane waves as described in the previous section. The idea is to convert the vector-type far field pattern to scalar one and make use of the MUSIC algorithm for scalar waves with some modifications. We first briefly recall the classical MUSIC algorithm for scalar waves with far field measurements in the next subsection.

3.1 MUSIC algorithm for scalar waves

Consider the scattering of acoustic wave by point-like scatterers associated with incident plane wave $u^i(x,\theta) = e^{ikx\cdot\theta}$, where k is the wave number and $\theta \in \mathbb{S}^{n-1}$ is the direction of incidence. Then under the assumption of weak scattering, it follows from (6) that the far field pattern can be given by [19]

$$u^{\infty}(\hat{x},\theta) = \sum_{m=1}^{M} \tau_m e^{iky_m\cdot(\theta-\hat{x})}, \hat{x}\in\mathbb{S}^{n-1}. \tag{14}$$

The MUSIC algorithm is to determine the locations y_m, $m = 1,2,\ldots,M$, of the scatterers from measured far field pattern $u^{\infty}(\hat{x},\theta)$ for a finite set of incidence and scattered directions, i.e., $\hat{x},\theta \in \{\theta_j, j = 1,\ldots,N\} \subset \mathbb{S}^{n-1}$. Here we assume that the number of scatterers is not larger than the number of incidence (and observation) directions, i.e., $N \geq M$. Given the measured far field pattern, we define the multistatic response matrix

$F \in \mathbb{C}^{N\times N}$ by

$$F_{j,l} = u^\infty(\theta_j, \theta_l) = \sum_{m=1}^{M} \tau_m e^{iky_m\cdot(\theta_l-\theta_j)}. \tag{15}$$

In order to determine the locations y_m, we consider a grid of sampling points $z \in \mathbb{R}^n$. For each point z, we define the vector $\phi_z \in \mathbb{C}^N$ by

$$\phi_z = (e^{-ikz\cdot\theta_1}, e^{-ikz\cdot\theta_2}, \ldots, e^{-ikz\cdot\theta_N})^T. \tag{16}$$

The use of the MUSIC algorithm is based on the property that ϕ_z is in the range $R(F)$ of F iff z is at one of the locations of the scatterers. That is, $z \in \{y_1, y_2, \ldots, y_M\}$ iff $\mathcal{P}\phi_z = 0$, where $\mathcal{P}$ is the projection onto the null space $N(F^*) = R(F)^\perp$ of the adjoint matrix F^* of F ([19], chapter 4).

3.2 MUSIC algorithm for elastic waves

In applying the MUSIC algorithm for elastic waves, we have noticed that care must be taken in designing measurement setups as well as some modifications are needed in forming the multistatic response matrix. For example, if we use the P part of the far field patterns of the P incident plane waves, i.e., $u_p^{\infty,p}$, it is clear that the measured data vanishes in the directions orthogonal to the incidence direction θ. That is, the measured data in these directions are useless. More generally, the information contained in the far field patterns is proportional to $|\hat{x}\cdot\theta|$ - the cosine of the angle between the incidence and observation directions. Therefore, to obtain usable data, the measurement system should be set up in such a way that $|\hat{x}\cdot\theta| \geq \gamma > 0$.

With this system setup, given the P part of the far field patterns, we can calculate the scalar far field pattern

$$u^\infty(\hat{x},\theta) = \frac{u_p^{\infty,p}(\hat{x},\theta)\cdot\theta}{a_p(\hat{x}\cdot\theta)^2} = \sum_{m=1}^{M} \tau_m e^{ik_p y_m\cdot(\theta-\hat{x})}. \tag{17}$$

In this case, we can use the same algorithm as in the scalar case to find the locations of the scatterers, with ϕ_z in (16) being replaced by the test vector

$$\phi_z^p = (e^{-ik_p z\cdot\theta_1}, e^{-ik_p z\cdot\theta_2}, \ldots, e^{-ik_p z\cdot\theta_N})^T \tag{18}$$

which corresponds to the longitudinal far field of the P part of a point source located at z. The case of S incident waves and S part of the far field patterns is treated in the same way by using the test vector

$$\phi_z^s = (e^{-ik_s z\cdot\theta_1}, e^{-ik_s z\cdot\theta_2}, \ldots, e^{-ik_s z\cdot\theta_N})^T. \tag{19}$$

which represents the transversal far field of the S part of the point source.

Now consider the mixed cases, i.e., S incident waves and P part of the far field patterns or P incident waves and S part of the far field patterns. By similar arguments as above, we note that the observation directions should not be parallel or anti-parallel to the incidence directions. In these cases, modifications are needed in applying the MUSIC algorithm since we have the presence of both S and P wavenumbers k_s and k_p. Indeed, let us consider the former case. Similar to the above case, we assume that $|\hat{x} \cdot \theta^{\perp}| \geq \gamma > 0$. Under this assumption, we can calcuate from the P far field pattern (12) the following *modified* multistatic response matrix $\tilde{F} \in \mathbb{C}^{N \times N}$ by

$$\tilde{F}_{j,l} = \sum_{m=1}^{M} \tau_m e^{ik_s y_m \cdot \theta_l} e^{-ik_p y_m \cdot \hat{x}_j} \tag{20}$$

with $\theta_l, l = 1, \ldots, N$, being the directions of incidence and $\hat{x}_j, j = 1, \ldots, N$, the observation directions. Note that this modified multistatic response matrix is different from the scalar one due to the presence of two different S wavenumber k_s and P wavenumber k_p. Following the same arguments as in [19], we factorize the matrix $\tilde{F}$ as

$$\tilde{F} = H^{p*} T H^{s}, \tag{21}$$

where H^p and H^s are matrices in $\mathbb{C}^{M \times N}$ defined by

$$H^p_{mj} = \sqrt{|\tau_m|} e^{ik_p y_m \cdot \hat{x}_j}, \; H^s_{mj} = \sqrt{|\tau_m|} e^{ik_s y_m \cdot \theta_j}, m = 1, \ldots, M; j = 1, \ldots, N. \tag{22}$$

The square matrix T is given by $T = \mathrm{diag}(\mathrm{sign}\tau_m)$ with $\mathrm{sign}\tau_m = \tau_m/|\tau_m|$.

It follows from (21) that

$$\tilde{F}^* \tilde{F} = H^{s*} \tilde{T} H^{s}, \tag{23}$$

with $\tilde{T} = T^* H^p H^{p*} T$.

Now for each sampling point $z \in \mathbb{R}^n$, we also make use of the test vector ϕ^s_z defined by (19). As in the scalar case, the key properties of the MUSIC algorithm are: (i) the vector ϕ^s_z belongs to $R(H^{s*})$ iff $z \in \{y_1, \ldots, y_M\}$ and (ii) the range $R(\tilde{F}^* \tilde{F})$ of $\tilde{F}^* \tilde{F}$ coincides the range $R(H^{s*})$ of H^{s*}. They are proved in the following theorem.

Theorem 3.1. *Suppose that the sets $\{\theta_n, n \in \mathbb{N}\} \subset \mathbb{S}^{n-1}$ and $\{\hat{x}_n, n \in \mathbb{N}\} \in \mathbb{S}^{n-1}$ are dense on $\mathbb{S}^{n-1}$ in the sense that any analytic function on $\mathbb{S}^{n-1}$ that vanishes on one of these sets vanishes on the whole $\mathbb{S}^{n-1}$. Let K be a compact set of $\mathbb{R}^n$ containing $\{y_m, m = 1, \ldots, M\}$. Then there exists a number $N_0 \in \mathbb{N}$ such that for all $N \geq N_0$, the following properties are satisfied*

(i) $z \in \{y_1, y_2, \ldots, y_M\}$ iff $\phi^s_z \in R(H^{s*})$ for $z \in K$.

(ii) $R(\tilde{F}^* \tilde{F}) \equiv R(H^{s*})$.

Therefore, $z \in \{y_1, y_2, \ldots, y_M\}$ iff $\phi^s_z \in R(\tilde{F}^* \tilde{F})$ or equivalently, $\mathcal{P}\phi^s_z = 0$, where P is the projection onto the null space of the self-adjoint matrix $\tilde{F}^* \tilde{F}$.

Proof. The proof is essentially the same as that of Theorem 4.1 of [19]. The only difference is that in this case we make use of two different sets of incidence and observation directions. Using the same arguments as of the mentioned theorem, we can prove first that there exists a number $N_1 \in \mathbb{N}$ such that the vectors $\phi^s_{y_1}, \ldots, \phi^s_{y_M}, \phi^s_z$ are linearly independent for $N \geq N_1$ and $z \in K \setminus \{y_1, \ldots, y_M\}$ and the point (i) of the theorem exactly follows from the proof of Theorem 4.1 of [19].

Now consider the point (ii). It is clear from (21) that $R(\tilde{F}^*\tilde{F}) \subset R(H^{s*})$. Now assume that $y \in R(H^{s*})$. Then there exists $x \in \mathbb{C}^M$ such that $y = H^{s*}x$. The linear independence of $\phi^s_{y_1}, \ldots, \phi^s_{y_M}$ implies that the matrix H^s has maximal rank. Equivalently, H^s is surjective from $\mathbb{C}^N$ to $\mathbb{C}^M$.

Concerning the matrix H^p, we define the following vector

$$\tilde{\phi}^p_z = (e^{-ik_p z\cdot\hat{x}_1}, e^{-ik_p z\cdot\hat{x}_2}, \ldots, e^{-ik_p z\cdot\hat{x}_N})^T. \tag{24}$$

Following the same arguments of the point (i), we also can prove that there exists a number $N_2 \in \mathbb{N}$ such that the vectors $\tilde{\phi}^p_{y_1}, \ldots, \tilde{\phi}^p_{y_M}$ are linearly independent for $N \geq N_1$. That means, H^p has maximal rank. Therefore $\tilde{T}$ is invertible. Now for $N \geq N_0 = \max\{N_1, N_2\}$, there exists $\tilde{y} \in \mathbb{C}^N$ such that $x = \tilde{T}H^s\tilde{y}$ as H^s is surjective. That is $y = H^{s*}\tilde{T}H^s\tilde{y} \in R(\tilde{F}^*\tilde{F})$. The proof is complete. □

Remark 3.1. Instead of the test vector ϕ^s_z, we can also use the vector $\tilde{\phi}^p_z$ for the MUSIC algorithm. However, in this case, the matrix $\tilde{F}^*\tilde{F}$ must be replaced by $\tilde{F}\tilde{F}^*$.

4 Numerical results and discussions

In this section, we illustrate the performance of the MUSIC algorithm for elasticity using one type of wave and compare the results for the case of S and P incident plane waves. It is expected that, since they have shorter wavelength, the S incident waves should provide sharper results compared to the P incident waves. This is confirmed in the following numerical examples.

For the convenience in visualizing the results, we only show results for two dimensional problems. We should mention that the algorithm in two and three dimensional spaces are the same. But we are aware that the three dimesional case is a bit more complicated since there are two linearly independent directions for the transverse waves.

As we mentioned in the previous section, care must be taken in setting up the measurements to avoid small values of the measured far field patterns. For this purpose, we propose the following setups in two situations.

For P incident waves and P part of far field patterns (PP case), or S incident waves and S part of far field patterns (SS case) we should avoid perpendicular directions. Denote by N_d the number of incidence directions (angles) used in a quarter of the unit circle. In

the first and the third quarters, we use the following incidence angles (see Figure 1(a))

$$\begin{aligned}\theta_j &= (j-1)\frac{\pi}{2N_d},\\ \theta_{2N_d+j} &= \pi + (j-1)\frac{\pi}{2N_d}, j = 1,\ldots,N_d,\end{aligned}$$

and in the second and the fourth quarters, we make use of the incidence angles

$$\begin{aligned}\theta_{N_d+j} &= \frac{\pi}{2} + \frac{\pi}{4N_d} + (j-1)\frac{\pi}{2N_d},\\ \theta_{3N_d+j} &= \frac{3\pi}{2} + \frac{\pi}{4N_d} + (j-1)\frac{\pi}{2N_d}, j = 1,\ldots,N_d.\end{aligned}$$

The observation directions are taken the same as the incidence one. In this setup, we have $|\hat{x}\cdot\theta| \geq \sin(\frac{\pi}{4N_d})$ for all $\hat{x},\theta \in \{\theta_j, j = 1,\ldots,4N_d\}$.

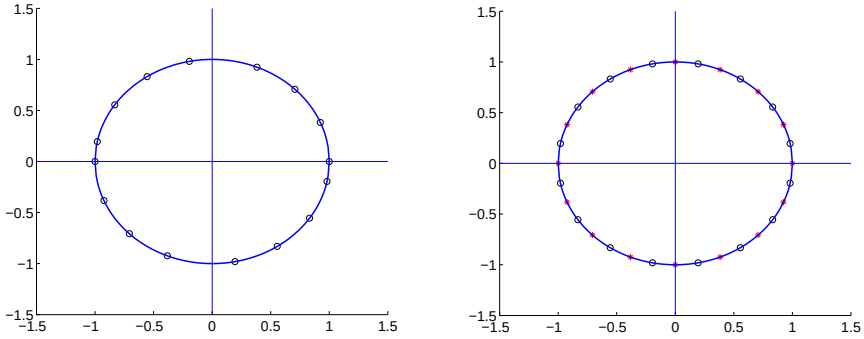

(a) (b)

Figure 1: Incidence and observation directions with $N_d = 4$: (a) PP and SS cases (the incidence and observations coincide); (b) PS and SP cases ('o': incidence directions, '*': observation directions)

To avoid parallel or anti-parallel directions in the case of P incidence waves and S part of far field patterns (PS case) or S incidence waves and P part of far field patterns (SP case), we choose the incidence and observation angles as follows (Figure 1(b)).

$$\begin{aligned}\theta_j &= (j-1)\frac{\pi}{2N_d}, j = 1,\ldots,4N_d,\\ \hat{x}_j &= \theta_j + \frac{\pi}{4N_d}, j = 1,\ldots,4N_d.\end{aligned}$$

With this choice, the minimum angle between the incidence and observation angles is $\frac{\pi}{4N_d}$.

In the following examples, the parameters are chosen as $\lambda = 2$, $\mu = 1$ and $k = 2\pi$ resulting in $k_p = \pi$ and $k_s = 2\pi$.

Let us first consider four point-like scatterers located at $y_1 = (0,0)$, $y_2 = (0,0.5)$, $y_3 = (1,1)$ and $y_4 = (1,-1)$. They have the same scattering strength of $\tau_m = 1, m = 1,\ldots,4$. In this case, the number of incidence directions is chosen to be $4N_d = 16$.

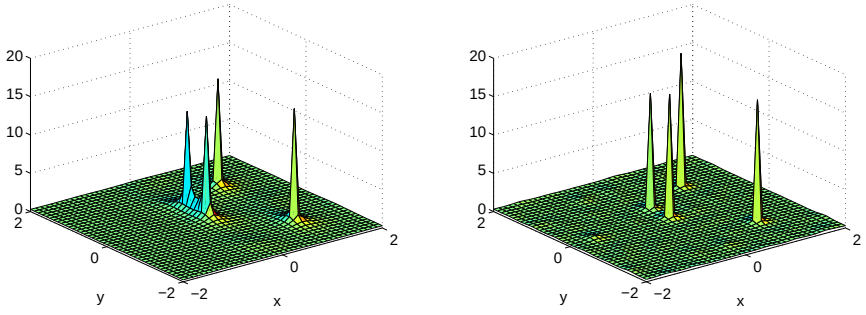

(a) (b)

Figure 2: Pseudo spectrum of 4 scatterers with 1% noise: (a) PP case; (b) SP case.

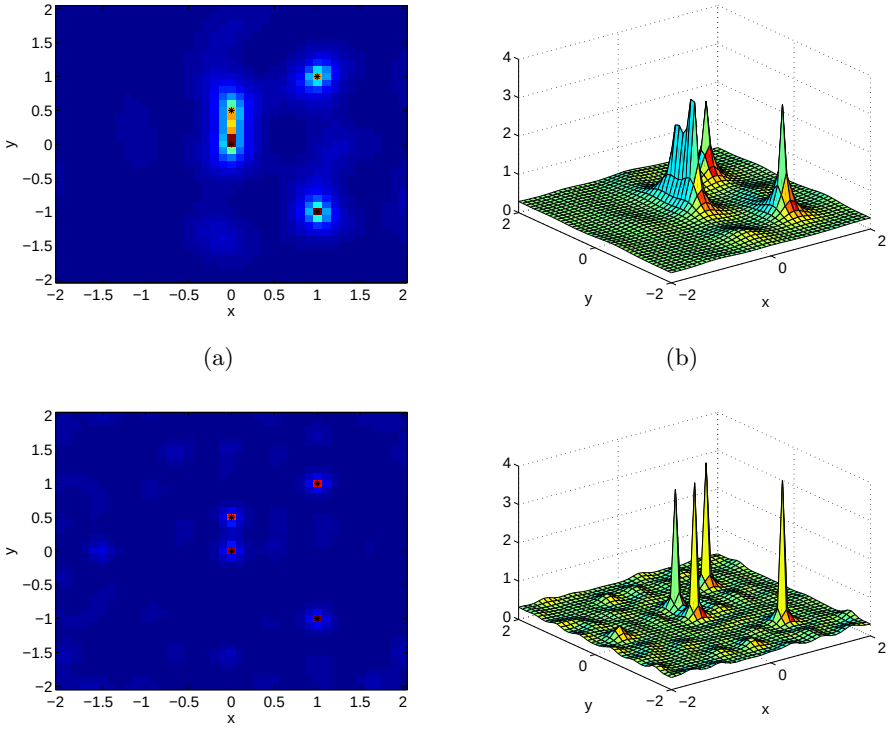

(a) (b)

(c) (d)

Figure 3: Pseudo spectrum of 4 scatterers with 5% noise: (a) and (b) PP case; (c) and (d) SP case. The stars '*' represent the locations of the scatterers.

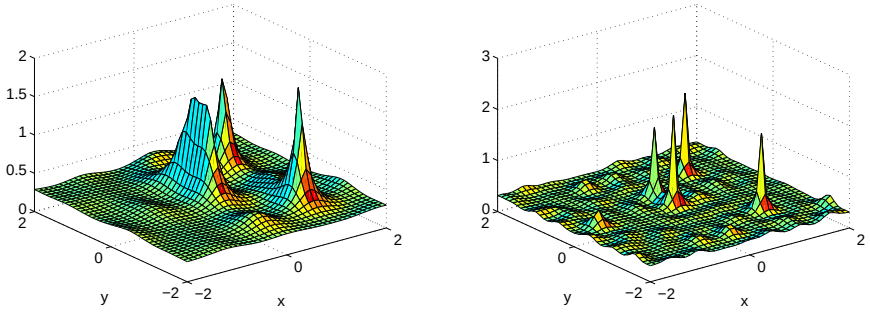

(a) (b)

Figure 4: Pseudo spectrum of 4 scatterers with 10% noise: (a) PP case; (b) SP case.

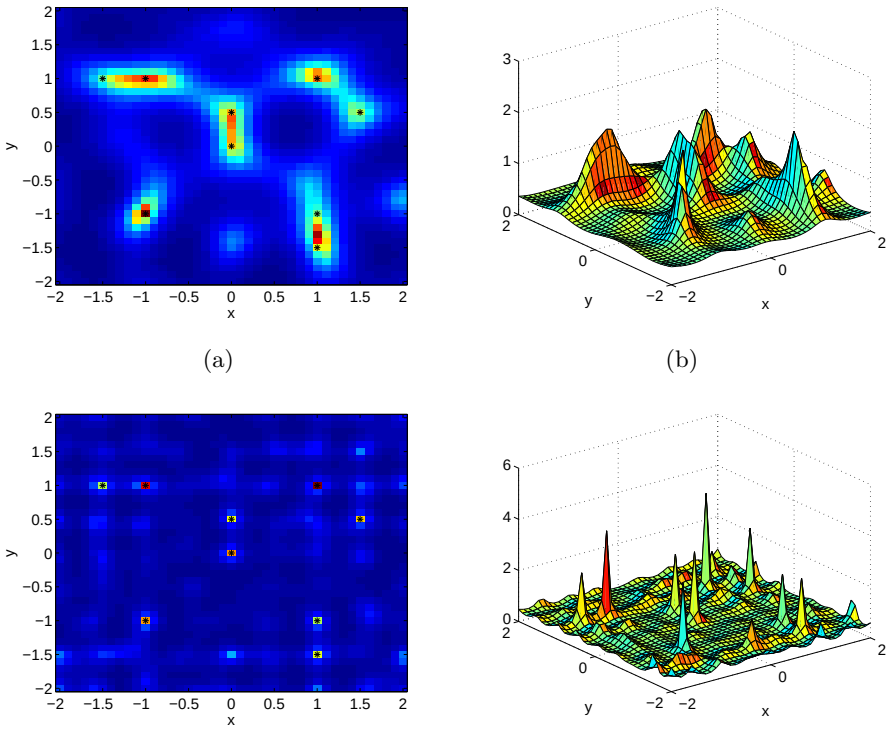

(a) (b)

(c) (d)

Figure 5: Pseudo spectrum of 9 scatterers with 5% noise: (a) and (b) PP case; (c) and (d) SP case. The stars '*' represent the locations of the scatterers.

Since the MUSIC algorithm is an exact method, see Theorem 3.1 (see also [19]), the reconstruction is very accurate if there is no noise in the measured data. In this paper, we concentrate on the resolution of the algorithm in case of noisy data. To analyze the effect of noise level on the resolution of the algorithm, different noise levels are used. Figures 2, 3 and 4 show the pseudo spectrum of the scatterers with 1%, 5% and 10% random noise in the measured far field patterns, respectively.

We should emphasize that, by converting from the vector far field patterns to the scalar one as in (17), the noise in the measured far field patterns is amplified in the modified multistatic response matrix resulting worse results than the scalar case.

Figure 2 shows good reconstructions for all scatterers in both PP and SP cases even though in the latter case the peaks are a bit sharper at the locations y_1 and y_2. In Figure 3, with 5% noise in the data, the two scatterers at y_1 and y_2 are not well separated anymore in the PP case but they are still very well separated in the SP case. The effect is more clear in Figure 4 with 10% noise. Here the two close scatterers are still clearly visible in the SP case but not anymore distinguishable in the PP case. These results show that using the S incident waves we can obtain better resolution with the MUSIC algorithm than using the P incident waves.

This phenomenon is more clearly visible when the number of scatterers increases. Indeed, Figure 5 shows that, with 9 scatterers, the scatterers close to each other (at the distance of about one fourth of the wavelength) are hardly or even impossible to be separated in the PP case although the noise level is only 5%, but they are still distinguishable in the SP case.

However, even in the SP case, the result is less accurate than the previous example of 4 scatterers. Actually, the higher the number of scatterers, the lower the accuracy in both cases.

Finally, we should mention that the reconstruction results depend on the choice of the signal and noise subspaces of the multistatic response matrix. For small measurement noise, these two subspaces are easy to choose since there is a clear cut in the distribution of the singular values of the multistatic response matrix. However, for large noise, the distribution of the singular values are smooth and it becomes more difficult to separate the singular values of the signal and noise subspaces, see Figure 6 for the PP case with 4 scatterers. In this paper, since we want to compare the PP and SP cases, the singular values were separated manually which is based on the true number of point-like scatterers.

Conclusion

As a conclusion, we can say that using the S incident waves provides more accurate reconstruction of the locations of point-like scatterers using the MUSIC algorithm compared to

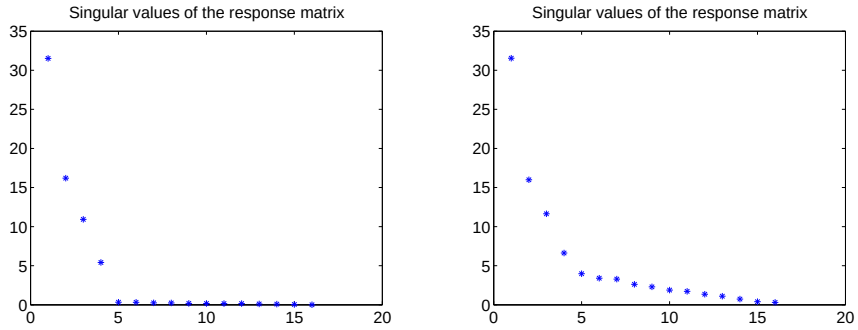

(a) (b)

Figure 6: The singular values of the modified multistatic response matrix in the PP case corresponding to 4 scatterers: (a) With 1% of noise; (b) With 10% of noise.

the P incident waves. Moreover, the larger the Lamé parameter λ, the better the reconstruction with the S incident waves compared to the P incident waves since, in this case, the wavelength of the P-incident wave is much larger than the one of the S-incident wave.

It is worth mentioning that from the numerical tests, we observed that the P and S parts of far field patterns, for a given incident wave, provide almost the same resolution. However, the magnitudes of the peaks may be different using P or S parts of the far field patterns. This may result in a better or worse reconstruction quality. Unfortunately, we are not able to quantify this property for the moment.

Acknowledgements

The authors thank the referees for their useful comments and suggestions for improving the paper. The work of Mourad Sini and Nguyen Trung Thành was supported by the Johann Radon Institute for Computational and Applied Mathematics (RICAM), Austrian Academy of Sciences and by the Austrian Science Fund (FWF) under the project No. P22341-N18. The work of Drossos Gintides was supported by the NTUA under the project PEBE 2010.

References

[1] C. Alves and H. Ammari. Boundary integral formulae for the reconstruction of imperfections of small diameter in an elastic medium. *SIAM J. Appl. Math.*, 62(1):94–106 (electronic), 2001.

[2] C. J. S. Alves and R. Kress. On the far-field operator in elastic obstacle scattering. *IMA J. Appl. Math.*, 67(1):1–21, 2002.

[3] H. Ammari, P. Calmon, and E. Iakovleva. Direct elastic imaging of a small inclusion. *SIAM J. Imaging Sci.*, 1(2):169–187, 2008.

[4] H. Ammari, P. Garapon, and F. Jouve. Separation of scales in elasticity imaging: a numerical study. *J. Comput. Math.*, 28(3):354–370, 2010.

[5] H. Ammari, P. Garapon, H. Kang, and H. Lee. A method of biological tissues elasticity reconstruction using magnetic resonance elastography measurements. *Quart. Appl. Math.*, 66(1):139–175, 2008.

[6] H. Ammari, J. Garnier, H. Kang, M. Lim, and K. Sølna. Multistatic imaging of extended targets. *SIAM J. Imaging Sci.* To appear.

[7] H. Ammari, H. Kang, G. Nakamura, and K. Tanuma. Complete asymptotic expansions of solutions of the system of elastostatics in the presence of an inclusion of small diameter and detection of an inclusion. *J. Elasticity*, 67(2):97–129, 2002.

[8] T. Arens. Linear sampling methods for 2D inverse elastic wave scattering. *Inverse Problems*, 17(5):1445–1464, 2001.

[9] K. Baganas, B. B. Guzina, A. Charalambopoulos, and G. D. Manolis. A linear sampling method for the inverse transmission problem in near-field elastodynamics. *Inverse Problems*, 22(5):1835–1853, 2006.

[10] A. Charalambopoulos, D. Gintides, and K. Kiriaki. The linear sampling method for the transmission problem in three-dimensional linear elasticity. *Inverse Problems*, 18(3):547–558, 2002.

[11] A. Charalambopoulos, D. Gintides, and K. Kiriaki. The linear sampling method for non-absorbing penetrable elastic bodies. *Inverse Problems*, 19(3):549–561, 2003.

[12] A. Devaney. Super-resolution processing of multi-static data using time reversal and music. Technical report, Northeastern University, 2000.

[13] D. Gintides and K. Kiriaki. The far-field equations in linear elasticity—an inversion scheme. *ZAMM Z. Angew. Math. Mech.*, 81(5):305–316, 2001.

[14] D. Gintides and M. Sini. Identification of obstacles using only the scattered p-waves or the scattered s-waves.

[15] B. B. Guzina and A. I. Madyarov. A linear sampling approach to inverse elastic scattering in piecewise-homogeneous domains. *Inverse Problems*, 23(4):1467–1493, 2007.

[16] P. Hähner. A uniqueness theorem in inverse scattering of elastic waves. *IMA J. Appl. Math.*, 51(3):201–215, 1993.

[17] P. Hähner and G. C. Hsiao. Uniqueness theorems in inverse obstacle scattering of elastic waves. *Inverse Problems*, 9(5):525–534, 1993.

[18] H. Kang, E. Kim, and J.-Y. Lee. Identification of elastic inclusions and elastic moment tensors by boundary measurements. *Inverse Problems*, 19(3):703–724, 2003.

[19] A. Kirsch and N. Grinberg. *The factorization method for inverse problems*, volume 36 of *Oxford Lecture Series in Mathematics and its Applications*. Oxford University Press, Oxford, 2008.

[20] V. D. Kupradze. *Potential methods in the theory of elasticity*. Translated from the Russian by H. Gutfreund. Translation edited by I. Meroz. Israel Program for Scientific Translations, Jerusalem, 1965.

[21] V. D. Kupradze, T. G. Gegelia, M. O. Basheleĭshvili, and T. V. Burchuladze. *Three-dimensional problems of the mathematical theory of elasticity and thermoelasticity*, volume 25 of *North-Holland Series in Applied Mathematics and Mechanics*. North-Holland Publishing Co., Amsterdam, russian edition, 1979. Edited by V. D. Kupradze.

[22] E. Marengo and F. Gruber. Subspace-based localization and inverse scattering of multiply scattering point targets. *EURASIP Journal on Advances in Signal Processing*, 2007(17342):16 pages, 2007.

[23] P. A. Martin. *Multiple scattering*, volume 107 of *Encyclopedia of Mathematics and its Applications*. Cambridge University Press, Cambridge, 2006. Interaction of time-harmonic waves with N obstacles.

[24] G. Nakamura, R. Potthast, and M. Sini. Unification of the probe and singular sources methods for the inverse boundary value problem by the no-response test. *Comm. Partial Differential Equations*, 31(10-12):1505–1528, 2006.

[25] G. Nakamura and M. Sini. Obstacle and boundary determination from scattering data. *SIAM J. Math. Anal.*, 39(3):819–837, 2007.

[26] S. Nintcheu Fata and B. B. Guzina. Elastic scatterer reconstruction via the adjoint sampling method. *SIAM J. Appl. Math.*, 67(5):1330–1352 (electronic), 2007.

[27] F. Simonetti. Localization of pointlike scatterers in solids with subwavelength resolution. *Applied Physics Letter*, 89:094105, 2006.